KFKI
2/1968

MAGNETIC STRUCTURES AND EXCHANGE INTERACTIONS IN THE Mn-Pt SYSTEM

E. Krén, G. Kádár, L. Pál, J. Sólyom,
P. Szabó and T. Tarnóczi

HUNGARIAN ACADEMY OF SCIENCES
CENTRAL RESEARCH INSTITUTE FOR PHYSICS

BUDAPEST

MAGNETIC STRUCTURES AND EXCHANGE INTERACTIONS IN THE Mn-Pt SYSTEM

E. Krén, G. Kádár, L. Pál, J. Sólyóm
P. Szabó and T. Tarnóczi
Central Research Institute for Physics, Budapest, Hungary

Abstract

The magnetic structures and transformations in the ordered phases of the Mn-Pt system have been investigated in a wide concentration range by magnetic, x-ray and neutron diffraction methods. The properties of the $Mn_3Pt_{1-y}Rh_y$ and $Mn_{3-z}Fe_zPt$ systems have been also studied.

The triangular and the collinear antiferromagnetic structures both found in the Mn_3Pt phase, undergo a first-order transformation into each other at a critical value of the lattice parameter where the next nearest neighbour interaction changes sign. In the MnPt phase a simple antiferromagnetic structure occurs with the directions of the magnetic moments dependent on concentration and temperature. There is no direct connection between the anisotropy energy and the lattice dimensions. The $MnPt_3$ phase has simple ferromagnetic structure.

The measured transition temperatures are summarized in magnetic phase diagrams. The magnetic structures and transformations of the Mn-Pt system are explained by assuming nearest and next nearest neighbour interactions dependent on the interatomic distances. The magnetic phase diagram of the Mn_3Pt phase calculated in the molecular field approximation is in agreement with the experimental observations.

I. INTRODUCTION

The metals of the 3d transition series form with platinum intermetallic compounds of ordered Cu_3Au and CuAu-I lattice type. These alloys show both antiferromagnetic and ferromagnetic behaviour and their common feature is the existence of ordered magnetic moment on the Pt atoms in the ferromagnetic state.

In the Mn-Pt system the ordered intermetallic compounds occupy a considerable part of the phase diagram obtained by Raub and Mahler [1] from x-ray diffraction and microscopic studies. At room temperature the ordered Mn_3Pt, MnPt and $MnPt_3$ phases are stable in the 16-29 at% Pt, 33-60 at% Pt and 63-83 at% Pt concentration ranges, respectively. According to the neutron diffraction measurements reported by Sidhu et al. [2] in Mn_3Pt two antiferromagnetic structures, not specified in detail, with different Néel temperatures coexist. The comparable compound Mn_3Rh has a non-collinear, triangular antiferromagnetic structure [3] . The magnetic properties of MnPt alloys were investigated by Brun et al. [4] who observed, in addition to the basic antiferromagnetism, the presence of ferromagnetism below 600° K in samples with higher than 52 at% Pt. The magnetic structure at room temperature was found to be simple antiferromagnetic and the direction of the magnetic moment to depend on concentration [5-6] . At the stoichiometric concentration the lattice parameters a and c, measured at room temperature, are at a maximum and a minimum, respectively. The $MnPt_3$ alloy is ferromagnetic [7] .

Among the other intermetallic compounds of the 3d metals with platinum, Fe_3Pt, FePt, CoPt and $CoPt_3$ are ferromagnetic [8-11] , while CrPt and $CrPt_3$ have antiferromagnetic and ferrimagnetic structures, respectively [12]. The magnetic structure of $FePt_3$ is antiferromagnetic or ferromagnetic, depending on concentration and atomic ordering [13] . The magnetic measurements in these compounds were analysed and the signs of the exchange interactions estimated by Sato [14] on the basis of an Ising model of ferromagnetism.

In order to get some insight into the nature of the exchange interactions of the Mn-Pt system, an extensive study on all ordered phases of the system was peformed using magnetic, x-ray and neutron diffraction methods. The observation of an antiferromagnetic-antiferromagnetic /AF-AF/ transforma-

tion of first-order in Mn_3Pt [15-17] and the occurrence of a transformation associated with a turn of the magnetic moments with respect to the tetragonal axis in MnPt [18] have been already reported in short communications. The present paper gives a full account of the investigation covering a wide concentration range, including the results obtained for some ternary /pseudo-binary/ alloys based on Mn_3Pt.

II. EXPERIMENTAL

The magnetic structures and their transformations were investigated on binary $Mn_{3+x}Pt_{1-x}$, $Mn_{1+x}Pt_{1-x}$ and $Mn_{1+x}Pt_{3-x}$ as well as on ternary / pseudo-binary/ $Mn_3Pt_{1-y}Rh_y$ and $Mn_{3-z}Fe_zPt$ alloys with different concentrations x, y and z.

The alloys were prepared in argon atmosphere by melting metals of 99,9 % purity in induction furnace. For magnetic measurements bulk specimens, for diffraction studies fine powders obtained by filing were used. To get the ordered phases the specimens were annealed in quartz tubes evacuated to 10^{-4} Torr. The initially long annealing /80-120 h/ at 700-800° C was later reduced to 2-3 h, since at this temperature range this proved to be sufficient for removing the effect of cold-working and for the ordering process. X-ray diffraction showed highly ordered homogeneous phases, with lattice parameter values listed in Tables I-III, V and VII, in all annealed samples but $Mn_{1+x}Pt_{1-x}$ with x=0,32 which was found to be contaminated by a trace of Mn_3Pt phase. In the ternary and non-stoichiometric binary alloys a substitutional disorder occurs on the sublattice containing two components. In the $Mn_{3-z}Fe_zPt$ system only samples with z lower than 0,7 were investigated, since alloys with higher values of z were inhomogeneous. The composition of the ingots was checked by chemical analysis which was repeated when a loss in weight due to annealing was observed. The results of the chemical analysis are included in Tables I-III, V and VII. In Table III the compositions are specified since alloys with the desired concentrations could not be produced.

Samples of the Mn_3Pt type were found to have disordered face-centred cubic structure after filing. The magnetic structure of this phase was investigated and reported earlier [19].

The magnetic measurements were made by magnetic balance in the range from liquid nitrogen temperature up to 800° C. The samples for the high temperature experiments were sealed in quartz ampules at a pressure of 10^{-4} Torr.

For the room temperature x-ray diffraction studies a Debye-Scherrer camera with CrKα radiation was used, while for high temperatures, up to 900° C, a furnace filled with 30 % H_2 and 70 % N_2 gas mixture and mounted on a Philips diffractometer was applied.

The neutron diffraction measurements from liquid helium temperature up to 800° C at 10^{-4} Torr pressure were performed by the automatically controlled diffractometer. Part of the neutron diffraction measurements reported earlier [15] was repeated with increased neutron flux available owing to the reconstruction of the reactor.

III. POSSIBLE MAGNETIC STRUCTURES

The Landau-theory of the second-order phase transformations [20] makes it possible to investigate the change in symmetry during a second-order transformation, thus to determine the magnetic structures which can arise from the paramagnetic phase in a single second-order transformation [21]. In this method the magnetic moment density $\underline{M}(r)$ of the system is expressed by the basic functions $\psi_j^{(l)}$ of the irreducible representations of the symmetry group in the paramagnetic phase, as

$$\underline{M}(r) = \sum_{\alpha,j,l} c_{\alpha,j}^{(l)} \, e_\alpha \psi_j^{(l)}(r) \qquad (1)$$

where e_α $/\alpha = x,y,z/$ is the axial vector in the direction α. The free energy of the system, which must be invariant under the symmetry transformations, can be given by invariant expressions constructed from the coefficients $c_{\alpha,j}^{(l)}$, of the form

$$\phi = \phi_0 + \sum_\alpha A_\alpha f^{(2)}(c_{\alpha,j}^{(l)}) + \sum_\beta B_\beta f^{(4)}(c_{\alpha,j}^{(l)}) + \ldots \qquad (2)$$

where $f^{(2)}(c_{\alpha,j}^{(l)})$ and $f^{(4)}(c_{\alpha,j}^{(l)})$ are the invariants of second and fourth order, respectively, while A_α and B_β are temperature dependent coefficients. The values of $c_{\alpha,j}^{(l)}$ can be determined by minimization of the free energy for the actual crystal structure and thus, by making use of the known irreducible representations, the spatial distribution of the magnetic moment can be obtained from equation (1).

Since these calculations seem to be very promising for the interpretation of neutron diffraction data, they were carried out for the magnetic unit cell dimensions inferred from the measurements. The results are shown for Mn_3Pt of cubic Cu_3Au structure in Fig. 1 for magnetic unit cells coinciding with the paramagnetic one and doubled in the direction z, while those for MnPt of tetragonal CuAu-I structure, with magnetic unit cell of the same size as the C-centred paramagnetic Bravais cell, are to be seen in Fig. 2.

As apparent from the figures, the possible configurations and directions of the magnetic moments are strictly prescribed by symmetry. At the same time, the possibility of any moment on the Pt atoms is also determined which is of great importance considering the experimental difficulties in establishing the existence of small moments.

There are four possible configurations, models A-D in Fig. 1, for Mn_3Pt if the size of the unit cell remains unchanged. In model A both Mn and Pt atoms may have magnetic moments arranged ferromagnetically and pointing in either [100] , [110] or [111] directions. The structure is ferromagnetic or ferrimagnetic, depending on the relative directions of the moments on Mn and Pt atoms. In model B one of the three Mn atoms of the unit cell has no magnetic moment while the moments on the other two are aligned antiferromagnetically in direction [101] . The magnetic moments in models C and D have triangular configuration. C is purely antiferromagnetic, no magnetic moment is allowed on the Pt atoms and the moments on the Mn atoms are confined to the (111) plane pointing in [110] directions /directions of the face-diagonals/. In D, besides the triangular component in the (111) plane pointing in [112] directions /in the centre of the triangle/, a ferromagnetic component normal to the (111) plane is allowed on both Mn and Pt atoms. If the ferromagnetic component is zero, the structure is antiferromagnetic and differs from model C only in the direction of the moment within the (111) plane, if the triangular component is zero, the structure coincides with model A.

Four antiferromagnetic structures, models E-H in Fig. 1, are allowed in the unit cell doubled in direction z. A common feature of these configurations is that part of the Mn atoms have no magnetic moment. The magnetic moments may point in the direction of axis z /as illustrated in the figure/ or in the directions [100] or [110] of the x-y plane. Magnetic moment on the Pt atoms is allowed only in models G and H.

Four configurations, models I-IV in Fig. 2, are possible for MnPt with magnetic unit cell coinciding with the C-centred paramagnetic Bravais cell. Model I is ferromagnetic with magnetic moments pointing in either [100] or [110] directions of the basal plane or the direction of the tetragonal axis. The Pt atoms may have magnetic moments, too. Models II-IV are antiferromagnetic with the same possible directions of the moment as those in the ferromagnetic case. No moment on the Pt atoms is allowed in model II.

The neutron diffraction measurements described in the next section will be interpreted by using the structures of Figs. 1-2.

IV. RESULTS

1. Mn_3Pt Phase

The magnetic properties of the Mn_3Pt phase were studied by observing the effect of the deviation from stoichiometry in the $Mn_{3+x}Pt_{1-x}$ system as well as that of the substitution of Rh for Pt and Fe for Mn in the $Mn_3Pt_{1-y}Rh_y$ and $Mn_{3-z}Fe_zPt$ systems. The results obtained on these samples are treated together.

a. Magnetic Structures

The temperature dependence of the magnetic susceptibility is shown in Fig. 3 for some typical samples of different compositions. An abrupt change in the susceptibility occurs at temperatures depending on concentration in the samples with $x < 0{,}18$ and $y < 0{,}2$. The change is accompanied by thermal hysteresis indicating a phase transformation. A maximum in the susceptbility can be observed, at temperatures depending again on concentration, only for $x \geq 0{,}18$, $y \geq 0{,}2$ and for all investigated values of z, when the abrupt change does not occur. The low values of the susceptibility and their independence of the magnetic field strength suggest pure antiferromagnetic state.

The neutron diffraction measurements were performed first at liquid nitrogen temperature. The diffraction patterns of all specimens are essentially the same consisting of reflections indexed in the unit cell of the Cu_3Au lattice. The temperature dependence of the intensities, given for reflection (110) in Fig. 4 for various values of x, show considerable magnetic contributions to the nuclear intensities. At the temperature of the abrupt change in susceptibility these magnetic contributions vanish suddenly with the simultaneous appearance of new reflections which can be indexed in a unit cell doubled in one direction. The variation of the neutron intensities exhibits thermal hysteresis, too. On further heating these new reflections also disappear, at temperatures depending again on concentration, which can be seen for $x=-0{,}17$ in Fig. 5 for the reflection indexed as $(10\frac{1}{2})$ in the original or (101) in the doubled unit cell. Above these temperatures no magnetic scattering can be detected in the neutron diffraction patterns. The abrupt change in the neutron intensities, the thermal hysteresis and the appearance of new reflections cannot be observed for $x \geq 0{,}18$, $y \geq 0{,}2$ and for all investigated values of z, the magnetic contributions to the nuclear reflections vanish smoothly in these cases at a temperature corresponding to that of the maximum in susceptibility.

A transformation from an ordered magnetic structure with unit cell of the same size as the paramagnetic one into another with a unit cell

doubled in one direction is seen to occur on increasing the temperature in samples with $x < 0{,}18$ and $y < 0{,}2$ while on continued heating a further transformation, now into the paramagnetic state, takes place. In the rest of the samples the low temperature structure undergoes a transformation directly into the paramagnetic state. In order to establish the magnetic structures, the structure factors of the models shown in Fig. 1 have to be evaluated and compared with the experimental intensities. Considering the susceptibility results, only the pure antiferromagnetic models have to be taken into account.

The magnetic structure factors for a collinear structure are given [22] by the expression

$$|F_{hkl}|^2 = \langle q^2_{hkl} \rangle \left| \sum_j p_j \exp(2\pi i \underline{k}\underline{r}_j) \right|^2 = \langle q^2_{hkl} \rangle |F'_{hkl}|^2 \qquad (3)$$

where p_j, $\underline{k}$ and $\underline{r}_j$ are the magnetic scattering amplitude, the reciprocal lattice vector and the atomic position vector, respectively. $q^2_{hkl} = \sin^2\alpha$ where α is the angle of the magnetic moment with respect to the [hkl] direction. The average of q^2_{hkl} for the polycrystalline case was calculated by Shirane [23]. For tetragonal symmetry, e.g.

$$\langle q^2_{hkl} \rangle = 1 - \frac{\ell^2 \left[\frac{1}{2}\left(\frac{c}{a}\right)^2 (h^2+k^2) - \ell^2\right] \sin^2\varphi_c}{\left(\frac{c}{a}\right)^2 (h^2+k^2) + \ell^2} \qquad (4)$$

where $\underline{a}$ and $\underline{c}$ are the lattice parameters of the tetragonal unit cell and φ_c is the angle of the magnetic moment with respect to the axis $\underline{c}$.

The structure factors of model B can be easily obtained from (3) as

$$|F_{hkl}|^2 = \frac{8}{3} p^2_{Mn} \qquad \text{for h,k,l mixed}$$

$$|F_{hkl}|^2 = 0 \qquad \text{for h,k,l unmixed}$$

The structure factors of the triangular models were evaluated by dividing the structure into three collinear substructures with tetragonal symmetry along the axes x, y and z.

$$|F_{hkl}|^2 = \sum_{i=x,y,z} \langle q^2_{hkl,i} \rangle |F'_{hkl,i}|^2 \qquad (5)$$

where the subscripts x, y and z refer to the substructures along the respective axes. $\langle q^2_{hkl,i} \rangle$ has the simple forms

$$\langle q^2_{hkl,x} \rangle = 1 - \frac{h^2}{h^2+k^2+\ell^2} \qquad \langle q^2_{hkl,y} \rangle = 1 - \frac{k^2}{h^2+k^2+\ell^2} \qquad \langle q^2_{hkl,z} \rangle = 1 - \frac{\ell^2}{h^2+k^2+\ell^2}$$

and the structure factors for model C are

$$|F_{hkl,x}|^2 = \frac{p_{Mn}^2}{2} \left| 1 - \exp[i\pi(k-\ell)] \right|^2$$

$$|F_{hkl,y}|^2 = \frac{p_{Mn}^2}{2} \left| 1 - \exp[i\pi(\ell-h)] \right|^2$$

$$|F_{hkl,z}|^2 = \frac{p_{Mn}^2}{2} \left| 1 - \exp[i\pi(h-k)] \right|^2$$

while for model D we have

$$|F_{hkl,x}|^2 = \frac{p_{Mn}^2}{6} \left| 2 - \exp[i\pi(h-k)] - \exp[i\pi(h-\ell)] \right|^2$$

$$|F_{hkl,y}|^2 = \frac{p_{Mn}^2}{6} \left| 2 - \exp[i\pi(k-h)] - \exp[i\pi(k-\ell)] \right|^2$$

$$|F_{hkl,z}|^2 = \frac{p_{Mn}^2}{6} \left| 2 - \exp[i\pi(\ell-h)] - \exp[i\pi(\ell-k)] \right|^2$$

As seen from these expressions, no magnetic reflections with h,k,l unmixed /all even or all odd/ occur. Since the structure factors for the nuclear scattering are

$$|F_{hkl}|^2 = (b_{Mn} - b_{Pt})^2 \qquad \text{for h,k,l mixed}$$

$$|F_{hkl}|^2 = (3b_{Mn} + b_{Pt})^2 \qquad \text{for h,k,l unmixed}$$

where b_{Mn} and b_{Pt} are the nuclear scattering amplitudes, the magnetic and nuclear scatterings appear together for all models in the reflections with mixed h,k,l .

The values of $\left| F'_{hkl} \right|^2$ obtained for models E–H in the doubled unit cell are summarized in Table IV, the values of $\langle q_{hkl}^2 \rangle$ are given by equation (4) with c=2a. As seen, the magnetic and nuclear reflections appear separately.

In the comparison of the calculated and measured structure factors of Corliss et al. [24] were used. In the ternary and non-stoichiometric binary alloys the scattering amplitudes have to be substituted for by an average corresponding to the actual concentrations.

At liquid nitrogen temperature good agreement can be obtained in all cases with model D except for $x > 0,09$ using the values of magnetic moment μ_{Mn} listed in Tables I-III. μ_{Pt} was taken to be zero according to the susceptibility results. The values of μ in Table III represent an average for the Mn and Fe atoms. When $x > 0,09$, model D cannot account for all the observed magnetic contributions to the nuclear intensities. This may be explained by the antiferromagnetic alignment of the magnetic moments of the excess Mn atoms on the Pt sublattice which tend to form a γ -Mn type antiferromagnetic order [25] in their environment. The observed and calculated intensities are in good agreement for the values of μ_{Mn} listed in Table I, assuming either the heterogeneous mixture, corresponding to the actual concentration, of D-type triangular and γ -Mn type collinear antiferromagnetic structures, or the homogeneous appearance of a γ -Mn type antiferromagnetic component normal to the plane of the triangle.

Above the transition temperature two magnetic superreflections, indexed as (101) and (103) in the doubled unit cell, can be measured in all specimens /Fig. 5/. A barely detectable additional (111) reflection was observed in the stoichiometric alloy only. As seen from Table IV, the absence of reflections with $l = 2n+1$ and $h-k = 2n$ is characteristic for model F. φ_c is evaluated from the measured (101) and (103) intensities as 90° in all cases, while for $x=0$ $\mu_{Mn}=3,4\pm0,3\,\mu_B$ at 384° K, for $x=0,07$ $3,7\pm0,3\,\mu_B$ at 340° K and for $x = -0,17$ $3,6\pm0,2\,\mu_B$ at 340° K were obtained. The appearance of the weak (111) reflection in the stoichiometric sample indicates an order, like that in models G and H, on the magnetically disordered sites of model F. The ordered moment on these sites, however, must be very small as compared with the values for model F. Thus, the basic magnetic structure above the transition temperature can be considered to be model F with magnetic moments lying in the plane normal to axis z.

b. Magnetic Structure Transformations

The Néel temperatures T_N for the collinear phase and T_N' for the triangular phase, when the collinear structure does not occur, as well as the temperature T_t of the transformation from triangular into collinear structure, defined as the centre of the hysteresis loop, were determined from the temperature variation of the neutron intensities and are given in Tables I-III. Due to the closeness of T_t and T_N, the latter could not be determined for the samples with $x=0,09$ and $y=0,1$. The values of T_N and T_N' marked in Fig. 3 are taken from the neutron diffraction measurements.

The abrupt variations accompanied by thermal hysteresis in the susceptibility and the neutron measurements suggest the transformation from triangular into collinear structure to be of first-order. Accordingly, the lattice parameter shows a discontinuous change at the transition temperature

T_t as seen in Fig. 6, where the temperature dependence of the lattice parameter, is given from x-ray diffraction measurements for typical alloys with various values of x and y. The magnitude of this discontinuity depends on concentration. In the transition range two discrete values of the lattice parameter, indicating the coexistence of the triangular and collinear phases, can be observed. At T_t the lattice parameter of the collinear phase has the same value, measured as $3{,}873 \pm 0{,}003$ Å, for all concentrations. This value seems to be critical. Below the Néel temperatures an anomaly in the thermal expansion is observed, the slope of the lattice parameter curve is seen to decrease below T_N for the collinear phase while to increase below T_N' for the triangular phase, with respect to the paramagnetic state. The magnitude of this anomaly depends on concentration, decreasing with increasing values of x, y and z.

The latent heat of the triangular-collinear transformation was found by Vincze [26] to be $1{,}7 \pm 0{,}2$ cal/g for Mn_3Pt.

2. MnPt Phase

The temperature dependence of the magnetic susceptibility in the 300-1100° K interval is shown in Fig. 7 for some typical alloys. The susceptibility exhibits characteristic antiferromagnetic variation with a break occurring at temperatures depending on concentration. Thermal hysteresis could not be observed, the susceptibility has low values even at liquid nitrogen temperature.

The neutron diffraction patterns at room temperature consist of reflections which can be indexed in the C-centred Bravais cell of the CuAu-I structure. Thus, to determine the magnetic structure, the structure factors have to be calculated for the models given in Fig. 2. According to the susceptibility results only the antiferromagnetic models II-IV have to be taken into account. The values of $\left|F'_{hkl}\right|^2$ are given in Table VI for $x=0$ in the $Mn_{1+x}Pt_{1-x}$ system, while those of $\langle q^2_{hkl} \rangle$ can be obtained from equation (4). In cases of $x \neq 0$ the amplitudes have to be substituted for by an average corresponding to the actual concentration. As seen, the nuclear and magnetic reflections appear separately. The structure factors for models III and IV coincide and are different from those for model II only in the values of $\langle q^2_{hkl} \rangle$ when the Pt atoms have no moment. Good agreement can be obtained between the neutron intensities calculated and measured at room temperature by taking the values of μ_{Mn} and φ_c as listed in Table V and by assuming $\mu_{Pt}=0$. The values of μ_{Mn} at liquid helium temperature are, within the experimental accuracy, the same as those in Table V. $\varphi_c = 0°$

corresponds to model II, while $\varphi_c = 90^\circ$ to models III and IV between which it is not possible to decide by powder diffraction method. For samples with $x > 0$ the antiferromagnetic ordering of the excess Mn atoms in the sublattice of Pt is possible if $\varphi_c = 90^\circ$. In this case these Mn atoms contribute to the coherent magnetic scattering, too, thus μ_{Mn} may be somewhat lower than the values in Table V, i.e., $\mu_{Mn}=3,4\pm0,2\ \mu_B$, $3,4\pm0,3\ \mu_B$ and $3,5\pm0,2\mu_B$ for x = 0,24, 0,28 and 0,32, respectively. It cannot be decided, within the experimental accuracy, whether the excess Mn atoms are magnetically ordered or not.

On increasing the temperature, the neutron intensities reveal a transformation of structure II into structure III in two narrow concentration ranges near x=0 and 0.24. Between these two ranges the alloys have structure II while in any other range structure III prevails from 5° K up to the Néel temperature. The transformation can be easily followed up by measuring the temperature variation of the (100) and (101) magnetic reflections, since during the transformation $\langle q^2_{100} \rangle$ changes from 1,00 to 0,50, while $\langle q^2_{101} \rangle$ from 0,48 to 0,77, altering the integrated intensity ratio I_{100}/I_{101} from 4 to 1. This is illustrated in Fig. 8 for x=0. The transformation takes place in a wide temperature range the centre of which is taken to be the transition temperature T_S. No thermal hysteresis can be observed. The temperature dependence of the (100) reflection is given for various alloys in Fig.9, the values of T_S and T_N, as obtained from these curves, are included in Table V. The simultaneous investigation of the nuclear intensities showed no change in the atomic ordering in the temperature interval involved. The susceptibility curves of Fig. 7 show the break at temperatures corresponding to the Néel temperature but do not exhibit any anomaly at T_S.

The temperature dependence of the lattice parameters was measured by x-ray diffraction and is given for x=0 in Fig. 10. Below the Néel temperature a well apparent anomaly can be seen. The magnitude of this anomaly decreases with deviation from the stoichiometry. The magnetic structure transformation does not affect the lattice parameters.

3. $MnPt_3$ Phase

The $Mn_{1+x}Pt_{3-x}$ system has simple ferromagnetic structure, the values of the magnetic moment on the Mn and Pt atoms were determined by Pickart and Nathans [7] for x=0.

The values of the Curie point T_C, as determined from the temperature dependence of the magnetization, are given in Table VII for various values of x. Above T_C the susceptibility obeys the Curie-Weiss law.

The temperature dependence of the lattice parameter does not show any anomaly below T_C.

V. DISCUSSION

1. Magnetic Structures

In our earlier reports [15-17] the combination of models F and G was suggested for the magnetic structure of Mn_3Pt above T_t in order to account qualitatively for the (101), (111) and (103) reflections observed but then not measurable to appropriate accuracy. The improved experimental conditions and the study of other compositions led to the refinement of the structure which turned out to be model F. The slight secondary ordering in the stoichiometric alloy, resulting in the weak (111) reflection, may be attributed to the effect of Mn atoms on the Pt sites due to a small atomic disorder. This effect is expected to be more significant when $x > 0$ but this could not be verified because of the closeness of T_t and T_N in these samples.

The magnetic structure established for Mn_3Rh is in agreement with the result of Kouvel and Kasper [3] but that for Mn_3Pt is inconsistent with the structures given by Sidhu et al. [2] . This discrepancy can be explained by their using a sample with $x < 0$ in which the AF-AF transformation takes place near to room temperature. Though aware of the coexistence of two structures, the authors did not determine them correctly and failed to recognize their transformation into each other.

The magnetic structures obtained at room temperature for the $Mn_{1+x}Pt_{1-x}$ alloys are in agreement with the results of Andresen et al. [5-6]. The structure is unambiguous only when $\varphi_c = 0^\circ$, while in the case of $\varphi_c = 90^\circ$ there are uncertainties about the existence of moments on the Pt sublattice and the direction of the moments in the basal plane.

The $MnPt_3$ phase has simple ferromagnetic structure in agreement with the earlier investigations [7] , the direction of the magnetic moments with respect to the crystallographic axes cannot be determined from powder diffraction measurements.

The value of the magnetic moment on the Mn atoms in the Mn_3Pt phase is not affected by the composition within the experimental accuracy. The values of the magnetic moment in the MnPt phase are consistent with those in other Mn alloys of similar type [27] and are a little higher than those in the Mn_3Pt phase. A decrease in the magnetic moment with increasing values of x in the $Mn_{1+x}Pt_{1-x}$ system is observed which may be attributed to the effect of intersublattice Mn-Mn interactions existing in alloys with $x > 0$.

The susceptibility in the Mn_3Pt phase behaves unusually. No maximum can be observed at the T_N of the collinear-paramagnetic transformation, though it appears in the triangular-paramagnetic transformation. Above the Néel temperature the susceptibility does not obey the Curie-Weiss law. The anomalous behaviour of the susceptibility in the collinear phase may be, perhaps, attributed to the presence of magnetically disordered Mn atoms.

In the MnPt phase our susceptibility results are consistent with the Néel temperatures obtained from neutron diffraction but are inconsistent with the reported magnetic data [4-6]. The observed ferromagnetism in these earlier studies may be attributed to impurities, probably the ferromagnetic Mn_2Pt_2O of cubic Fe_4N type, the formation of which in the presence of air was observed by Yokoyama and Wuttig [28] . Similar effect of impurities was observed in other Mn alloys of similar type [27] .

The stability regions of the various magnetic structures can be seen in Figs. 11-12 where the magnetic phase diagrams, constructed from the measured transition temperature data, are shown for the systems Mn-Pt and $Mn_3Pt_{1-y}Rh_y$. For completeness, the Néel temperatures of the disordered face-centred cubic solid solutions [19] and pure γ-Mn [25] are also included.

2. Interpretation of the Phase Diagrams

a. Mn_3Pt Region

The anomalous thermal expansion occurring below the Néel temperatures /Fig. 6/ indicates exchange interactions dependent on the atomic distances. The increased thermal expansion below T_N' of the triangular phase suggests that the exchange energy decreases with decreasing interatomic separation indicating an effective interaction J_{eff}, the absolute value of which increases with decreasing interatomic separation. The opposite anomaly below T_N of the collinear phase implies a $|J_{eff}|$ increasing with increasing interatomic separation. Considering the magnetic structures, it can be assumed that the effective interaction is composed of the nearest neighbour J_1 and the next nearest neighbour J_2 Mn-Mn interactions.

Assuming nearest and next nearest neighbour interactions, the magnetic phase diagram can be calculated in the molecular field approximation using the method of Tahir-Kheli et al. [29] . The results for the Mn_3Pt lattice are given in Fig. 13. All possible structures with single, double, fourfold and eightfold unit cells, which are allowed by the symmetry to arise from the paramagnetic phase in a single second-order phase transformation, were taken into account. The stability regions of the respective structures

are denoted by letters referring to the models in Fig. 1. The regions of B, C and D coincide, structure K, not shown in Fig. 1, is collinear antiferromagnetic with an eightfold unit cell.

The molecular field phase diagram yields for the sign of the interactions in the triangular /structure D/ and collinear /structure F/ phases $J_1 < 0$, $J_2 > 0$ and $J_1 < 0$, $J_2 < 0$, respectively. The anomalous thermal expansion can be interpreted, if we locate these interactions, as shown in Fig. 13a, on a Bethe-Slater type qualitative curve [14] where the strength of the interaction is plotted against the ratio of the interatomic distance R to the 3d shell radius r. On increasing R in the triangular phase, both $|J_1|$ and $|J_2|$ thereby $|J_{eff}|$ decrease in accordance with the observations. In the collinear phase $|J_1|$ decreases while $|J_2|$ increases with increasing R, thus $|J_2|$ must be varying more strongly with R than $|J_1|$ to get the increase in $|J_{eff}|$ observed experimentally.

The molecular field phase diagram manifests the characteristic features of the experimental data. Points I-IV in Fig. 13 represent different values of the ratio $J_2/|J_1|$ in the triangular phase at 0° K. The increase in the temperature results in a displacement of these points along lines like 1-4, assuming the above dependence of J_1 and J_2 on the interatomic distances and a stronger variation of J_2. The magnetic transformations take place where these lines intersect the phase boundaries. The transformation from the triangular into the collinear structure /D→F/ occurs when $J_2=0$, which happens at a critical value of the lattice parameter, found experimentally as $3,873\pm0,003$ Å for the collinear phase. The theoretical phase diagram yields $kT/J_1S(S+1) = -8/3$ for the triple point P where $T=T_N=T'_N=T_t$. Taking the value of T from the experimental phase diagrams of Figs. 11-12 as $T=510\pm10^\circ$ K and taking $S=3/2$, the value of J_1 can be evaluated for Mn atoms, which are $d=3,873/\sqrt{2}=2,74$ Å apart, as $J_1=-51^\circ$ K.

The transformations in stoichiometric Mn_3Pt can be represented by a line similar to 3 in Fig. 13. On substituting Mn or Rh for Pt, i.e., on increasing concentrations x or y, a shift from point III towards I takes place at 0° K as a result of the contraction of the lattice due to the smaller atomic radii of the substitutes /see values of lattice parameter in Tables I-II/. Thus, the concentration dependence of each of the transition temperatures obtained from the theoretical phase diagram is in qualitative agreement with the experimental observations. There seems to be an inconsistency between the experiments and the molecular field model when we substitute Fe for Mn. Considering the room temperature data of Table III, which show an increase in the lattice parameter with increasing z, a shift from point III towards IV, i.e., a simultaneous decrease in T_t would be expected in

contrast with observation. However, the values of the lattice parameter at room temperature do not characterize the alloys since they are affected by the coefficient of and by the anomaly in the thermal expansion, both dependent on concentration. Thus, e.g., the data in Table III obtained by extrapolation from the paramagnetic state show an irregular sequence of the lattice parameter.The extrapolated values of the lattice parameter are given in Tables I-II and Fig. 6, too. Comparing the lattice parameters for $z = 0,4$ and $x=0,07$ with the same Pt concentration, it can be inferred that the substitution of Fe for Mn causes a contraction of the lattice thus an increase in T_t, as observed.

The measure of the discontinuity in the lattice parameter at T_t depends on the composition, varying from $\Delta a/a=8,0 \cdot 10^{-3}$ for $y=0$ to $1,5 \cdot 10^{-3}$ for $y=0,1$. This variation can be interpreted qualitatively by the schematic drawings inserted in Fig. 6. As the temperature decreases, the lattice parameter jumps at T_t from the curve of the collinear phase to that of the triangular phase. The distance between the two curves, i.e., the extent of the jump, decreases with increasing concentrations x and y, since it is determined by the spacing of T_t and T_N and by the magnitude of the anomalous thermal expansion, both decreasing with increasing concentrations x and y. The curves for the triangular phase in Fig. 6 are drawn by arbitrary dashed lines as far as the values of T_N' estimated from the phase diagrams of Figs. 11-12. These curves represent the temperature dependence of the lattice parameter for the triangular phase, assuming no AF-AF transformation to occur.

b. MnPt Region

The anomalous thermal expansion below the Néel temperature /Fig. 10/ can be explained by the same interatomic distance dependent interactions which we have assumed in the triangular phase of Mn_3Pt.

The lattice parameter a , i.e., the distance between the nearest neighbour Mn atoms, is at a maximum at the stoichiometric concentration, therefore a minimum in T_N might be expected, considering the decrease in $|J_1|$ with increasing interatomic distance. The values of T_N,however, show a maximum at $x=0$. The decrease in T_N for $x < 0$ may be regarded as a dilution effect in the Mn sublattice, while the stronger decrease for $x > 0$ may be attributed to the intersublattice Mn-Mn interactions which affect the value of the magnetic moment, too.

The structure transformation associated with the turn of the magnetic moments with respect to the tetragonal axis reflects a change in the magnetic anisotropy. In contrast with the similar Morin-transition in rhombohedral α-Fe_2O_3 [30] , the wide temperature range of the transition,

the lack of a discontinuity in the lattice parameter and the absence of thermal hysteresis seem to render it questionable whether this transformation is of first-order.

Considering the onset of the transformation in two separate ranges of concentration and the existence of extreme values of the lattice parameters at the stoichiometric concentration, observed by Brun et al. [4] and confirmed by the present study, a direct relation of the anisotropy energy to the lattice dimensions might be supposed. This would mean the assumption of critical values of the lattice parameters at which the anisotropy energy changes sign. This idea is, however, contradicted by the experimental data, showing such different values of the lattice parameters at T_t as a=4,03 Å , c=3,67 Å and c/a=0,911 for x=0 and a=3,93 Å, c=3,74 Å and c/a=0,951 for x=0,24. Furthermore, this assumption would result in a concentration dependence of the transition temperature T_s different from that observed. The present measurements do not permit to give any explanation of the transformation, for more information single crystal investigations would be needed.

c. $MnPt_3$ Region

No anomaly in the thermal expansion can be observed within the experimental accuracy. The variation of the Curie temperature with composition, however, indicates a next nearest neighbour ferromagnetic interaction J_2 near to $|J_2|$ of the triangular Mn_3Pt phase on the Bethe-Slater type curve /Fig. 13a/. On increasing concentration x in the $Mn_{1+x}Pt_{3-x}$ system, the lattice parameter decreases /Table VII/ resulting in an increase in J_2 and consequently in T_c. This effect is weakened by the presence of the nearest neighbour Mn-Mn interaction when $x > 0$, and strengthened by the dilution of the Mn sublattice when $x < 0$, thus the variation of T_c is not linear.

In the $MnPt_3$ region $J_2 > 0$ in spite of the fact that the lattice parameter is greater than $a_{critical}$ where J_2 changes sign in Mn_3Pt. This can be explained by assuming that the 3d shell radius r is smaller in Mn_3Pt than in $MnPt_3$.

The existence of localized moment on the Pt atoms is an evidence of ferromagnetic nearest neighbour Mn-Pt interaction in the $MnPt_3$ phase.

VI. CONCLUSIONS

1. The simple antiferromagnetic and ferromagnetic structures, established in the ordered phases of the Mn-Pt system, are produced by the nearest and next nearest neighbour Mn-Mn interactions which are sensitive to the interatomic distances. J_1 is negative while J_2 is positive or negative depending on the interatomic separation.

2. The triangular and collinear structures of the Mn_3Pt phases undergo a first-order transformation into each other at a critical value of the lattice parameter at which J_2 changes sign. At the transition temperature it was found that $J_1 = 51^6$ K. Both the triangular and collinear structures are slightly modified in samples with higher than stoichiometric Mn concentration.

3. A magnetic transformation, reflecting a change in the anisotropy energy, occurs in the MnPt phase. A direct relation of the anisotropy energy to the lattice dimensions could not be established.

VII. ACKNOWLEDGMENTS

The authors are indebted to Mr. G. Konczos for preparing the samples, to Mrs. K. Zámbó for chemical analysis and to Mr. C. Hargitai for valuable discussions.

REFERENCES

[1] E. Raub and W. Mahler, Z. Metallk. 46, 282 /19655/.

[2] S.S. Sidhu, K. D. Anderson and D.D. Zauberis, Bull.Am.Phys.Soc. 10, 352 /1965/.

[3] J.S. Kouvel and J.S. Kasper, Proceedings of the International Conference on Magnetism, Nottingham, 1964 /Institute of Physics and Physical Society, London, 1965/ p. 169.

[4] K. Brun, A. Kjekshus and W.B. Pearson, Phil.Mag. 10, 291 /1964/.

[5] A.F. Andresen, A. Kjekshus, R.Møllerud and W.B. Pearson, Phil.Mag. 11, 1245 /1965/.

[6] A.F. Andresen, A. Kjekshus, R. Møllerud and W.B. Pearson, Acta Chem. Scand. 20, 2529 /1966/.

[7] S.J. Pickart and R. Nathans, J. Appl.Phys. 33, 1336 /1962/.

[8] E. Krén and P. Szabó, Solid State Comm. 3, 371 /1965/.

[9] A. Kussmann and G.G. v. Rittberg, Z.Metallk. 41, 470 /1950/.

[10] B.van Laar, J.Phys. 25, 600 /1964/.

[11] F. Menziger and A. Paoletti, Phys.Rev. 143, 365 /1966/.

[12] S.J. Pickart and R. Nathans, J.Appl.Phys. 34, 1203 /1963/.

[13] G.E. Bacon and J. Crangle, Proc.Roy.Soc. A 272, 387 /1963/.

[14] H. Sato, J.Appl.Phys. 31, 327 S /1960/.

[15] E. Krén, G. Kádár, L. Pál, J. Sólyom and P. Szabó, Phys.Letters 20, 331 /1966/.

[16] E. Krén, G. Kádár, L. Pál and P. Szabó, J.Appl.Phys. 38, 1265 /1967/.

[17] E. Krén, P. Szabó, L. Pál, T. Tarnóczi, G. Kádár and C. Hargitai, J.Appl.Phys. /to be published/

[18] E. Krén, M. Cselik, G. Kádár and L. Pál, Phys.Letters 24A, 198 /1967/.

[19] E. Krén, Phys.Letters 21, 383 /1966/.

[20] L.D. Landau and E.M. Lifshitz, Statistical Physics, Pergamon Press, London, 1958.

[21] O.V. Kovalyov, Fiz.Tverdogo Tela /USSR/ 5, 3156 /1963/

[22] G.E. Bacon, Neutron Diffraction, Clarendon Press, Oxford, 1962.

[23] G. Shirane, Acta Cryst. 12, 282 /1959/.

[24] L.M. Corliss, N. Elliott and J.M. Hastings, Phys.Rev. 104, 924 /1956/.

[25] G.E. Bacon, I.W. Dunmur, J.H. Smith and R. Street, Proc.Roy.Soc. A 241, 223 /1957/.

[26] I. Vincze /private communication/

[27] L. Pál, E. Krén, G. Kádár, P. Szabó and T. Tarnóczi, J.Appl.Phys. /to be published/

[28] T. Yokoyama and M. Wuttig, Z. Metallk. 54, 308 /1963/.

[29] R.A. Tahir-Kheli, H.B. Callen and H. Jarrett, J.Phys.Chem.Solids 27, 23 /1966/.

[30] C.G. Shull, W.A. Strauser and E.O. Wollan, Phys.Rev. 83, 333 /1951/.

Table I

Values of the lattice parameter a at room temperature /as measured and as extrapolated from the paramagnetic state/, the magnetic moment μ_{Mn} at 77° K and the transition temperatures T_t, T_N and T'_N for samples in the $Mn_{3+x}Pt_{1-x}$ system.

x	a (Å)		μ_{Mn} (μ_B)	T_t ($^{\circ}$K)	T_N ($^{\circ}$K)	T'_N ($^{\circ}$K)
	meas.	extr.				
- 0,17	3,850	3,868	2,8 ± 0,3	315±10	430±10	-
- 0,07	3,844	3,862	3,4 ± 0,4	315±10	460±10	-
0	3,833	3,858	3,0 ± 0,3	365±10	475±10	-
0,09	3,827	3,854	3,2 ± 0,4	455±10	could not be measured	-
0,18	3,827		2,9 ± 0,4	-	-	510±10
0,28	3,822		3,2 ± 0,4	-	-	525±10

Table II

Values of the lattice paramter a at room temperature /as measured and as extrapolated from the paramagnetic state/, the magnetic moment μ_{Mn} at 77°K and the transition temperatures T_t, T_N and T_N' for samples in the $Mn_3Pt_{1-y}Rh_y$ system.

y	a (Å) meas.	a (Å) extr.	μ_{Mn} (μ_B)	T_t (°K)	T_N (°K)	T_N' (°K)
0	3,833	3,858	3,0±0,3	365±10	475±10	-
0,05	3,833	3,854	3,5±0,4	415±10	465±10	-
0,1	3,832	3,849	2,8±0,3	505±20	could not be measured	-
0,2	3,828	3,837	3,2±0,4	-	-	555±10
0,5	3,820	3,824	3,5±0,4	-	-	685±10
1	3,813		3,6±0,4	-	-	855±10

Table III

Values of the lattice parameter a at room temperature /as measured and as extrapolated from the paramagnetic state/, the magnetic moment μ at 77° K and the Néel temperature T_N' for samples in the $Mn_{3-z}Fe_zPt$ system.

Composition	a (Å)		μ (μ_B)	T_N' (°K)
	meas.	extr.		
$Fe_{0,21}Mn_{2,76}Pt_{1,03}$	3,829	3,843	2,4±0,4	455±10
$Fe_{0,41}Mn_{2,52}Pt_{1,07}$	3,833	3,846	2,9±0,4	415±10
$Fe_{0,60}Mn_{2,36}Pt_{1,04}$	3,836	3,844	2,6±0,4	425±10

Table IV

Values of $\left|F'_{hkl}\right|^2$ for models in a doubled unit cell of the Cu_3Au lattice. b_{Mn}, b_{Pt} are the nuclear and p_{Mn}, p_{Pt} the magnetic scattering amplitudes. The Miller indices refer to the doubled /tetragonal unit cell.

Model	$\ell = 2n+1$		$\ell = 2n$	
	$h-k = 2n$	$h-k = 2n+1$	$h-k = 2n$	$h-k = 2n+1$
E	$16p_{Mn}^2$	0	$4(3b_{Mn} + b_{Pt})^2$	$4(b_{Mn} - b_{Pt})^2$
F	0	$16p_{Mn}^2$	$4(3b_{Mn} + b_{Pt})^2$	$4(b_{Mn} - b_{Pt})^2$
G	$4(p_{Mn} - p_{Pt})^2$	$4(p_{Mn} + p_{Pt})^2$	$4(3b_{Mn} + b_{Pt})^2$	$4(b_{Mn} - b_{Pt})^2$
H	$4(p_{Mn} + p_{Pt})^2$	$4(p_{Mn} - p_{Pt})^2$	$4(3b_{Mn} + b_{Pt})^2$	$4(b_{Mn} - b_{Pt})^2$

Table V

Lattice parameters a and c, magnetic moment μ_{Mn} and its angle φ_c to axis c, as measured at room temperature and the values of the transition temperature T_S and the Néel temperature T_N in the $Mn_{1+x}Pt_{1-x}$ system

x	a(Å)	c (Å)	c/a	μ_{Mn} (μ_B)	φ_c (°)	T_S (°K)	T_N (°K)
-0,18	3,96	3,73	0,943	4,3±0,3	90	-	815±10
-0,10	3,97	3,73	0,940	4,2±0,2	90	-	905±20
-0,04	3,99	3,67	0,920	4,2±0,2	90	< 5	955±10
0	4,00	3,67	0,918	4,3±0,2	0	~ 715	975±10
0,04	3,99	3,67	0,920	4,2±0,2	0	~ 785	885±20
0,13	3,97	3,71	0,935	3,9±0,2	0	-	695±20
0,24	3,93	3,73	0,950	3,5±0,2	90	~ 175	500±10
0,28	3,93	3,74	0,952	3,5±0,3	90	-	490±10
0,32	3,91	3,75	0.960	3,6±0,2	90	-	485±10

Table VI

Values of $\left|F'_{hkl}\right|^2$ for models in the CuAu-I type lattice. b_{Mn}, b_{Pt} are the nuclear and p_{Mn}, p_{Pt} the magnetic scattering amplitudes.

Model	h,k,l unmixed	h,k,l mixed	
		h - k = 2n	h - k = 2n+1
II	$4(b_{Mn} + b_{Pt})^2$	$4(b_{Mn} - b_{Pt})^2$	$4\,p_{Mn}^2$
III	$4(b_{Mn} + b_{Pt})^2$	$4(b_{Mn} - b_{Pt})^2$	$4(p_{Mn}^2 + p_{Pt}^2)$
IV	$4(b_{Mn} + b_{Pt})^2$	$4(b_{Mn} - b_{Pt})^2$	$4(p_{Mn}^2 + p_{Pt}^2)$

Table VII

Lattice parameter a at room temperature and the ferromagnetic Curie point T_C for samples in the $Mn_{1+x}Pt_{1-x}$ system

x	a (Å)	T_c (^oK)
-0,14	3,900	355 ± 20
-0,06	3,899	425 ± 15
0,20	3,895	540 ± 15

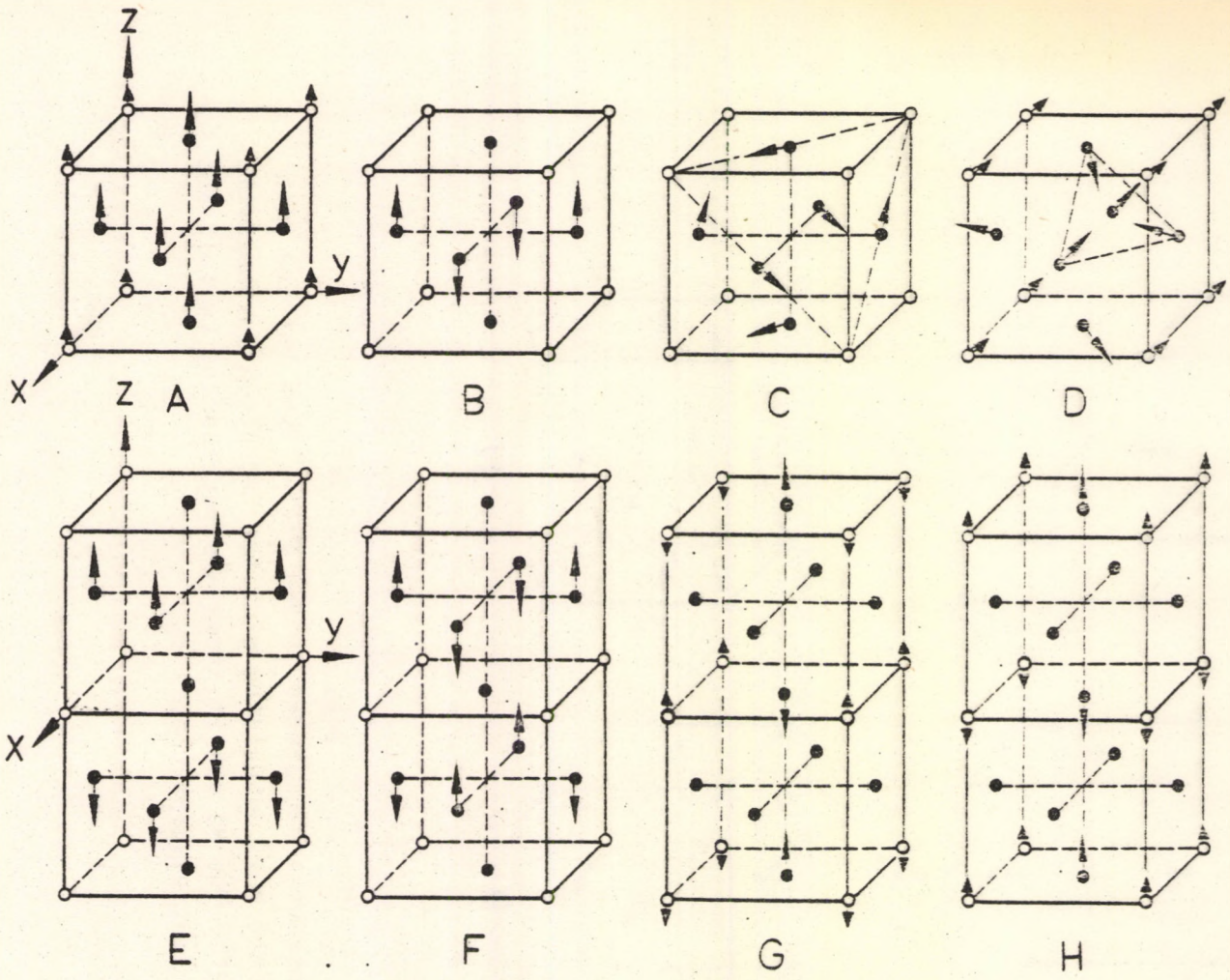

Fig. 1

Possible magnetic structures in the Cu_3Au type lattice with magnetic unit cells coinciding with the paramagnetic one /A-D/ and doubled in direction z /E-H/. The Mn and Pt atoms are represented by full and empty circles, respectively

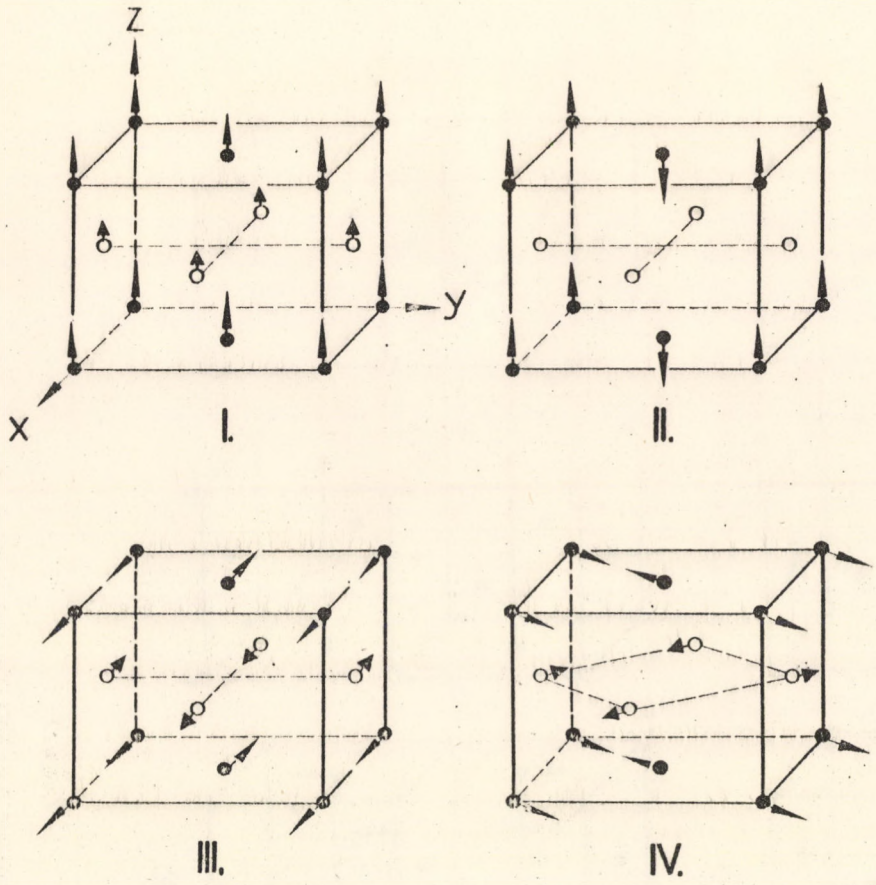

Fig. 2

Possible magnetic structures in the CuAu-I type lattice with magnetic unit cell coinciding with the C-centred paramagnetic Bravais cell. The Mn and Pt atoms are represented by full and empty circles, respectively

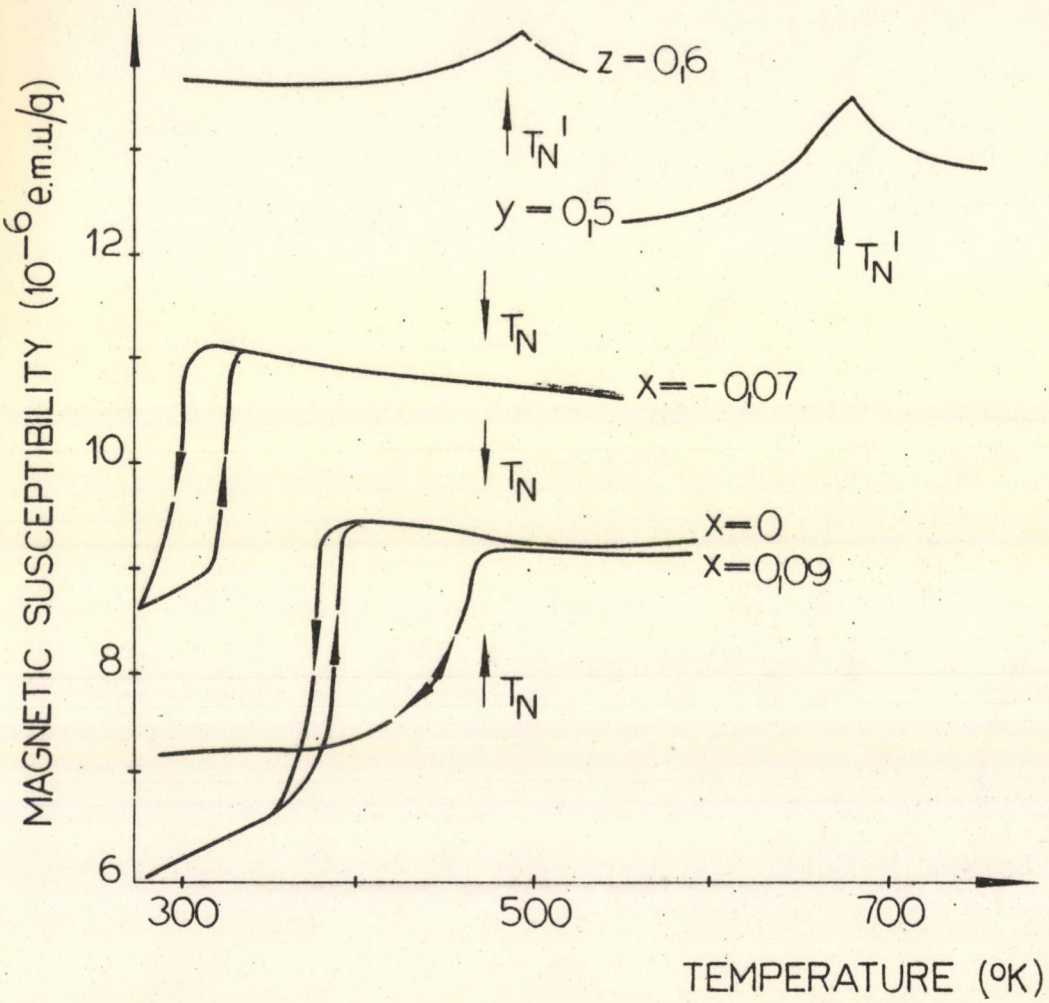

Fig. 3

Temperature dependence of the magnetic susceptibility for some typical samples in the systems $Mn_{3+x}Pt_{1-x}$, $Mn_3Pt_{1-y}Rh_y$ and $Mn_{3-z}Fe_zPt$. The values of T_N and T_N' marked in the figure were obtained by neutron diffraction

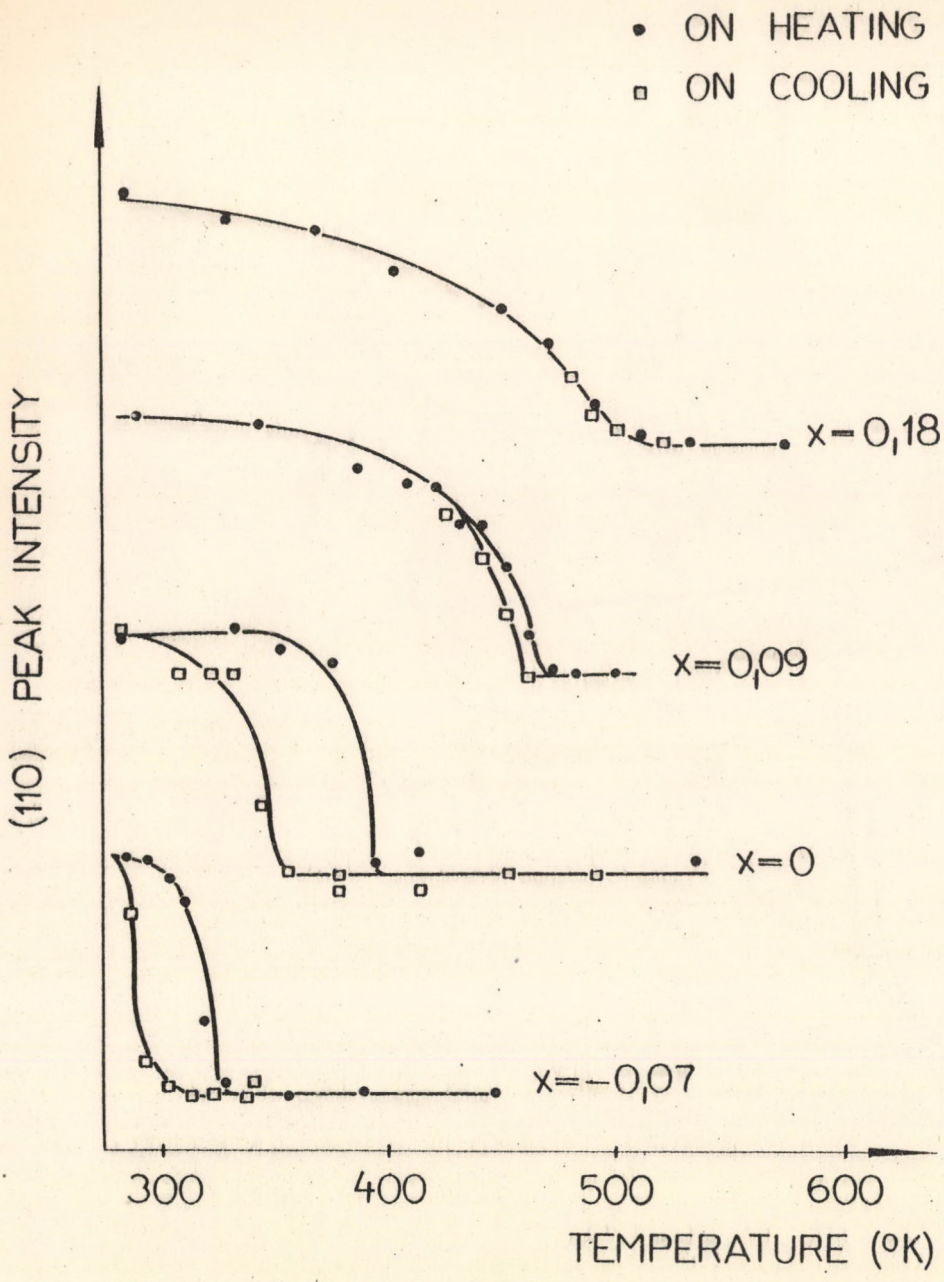

Fig. 4
Temperature dependence of the (110) peak intensity for different values of x in the $Mn_{3+x}Pt_{1-x}$ system

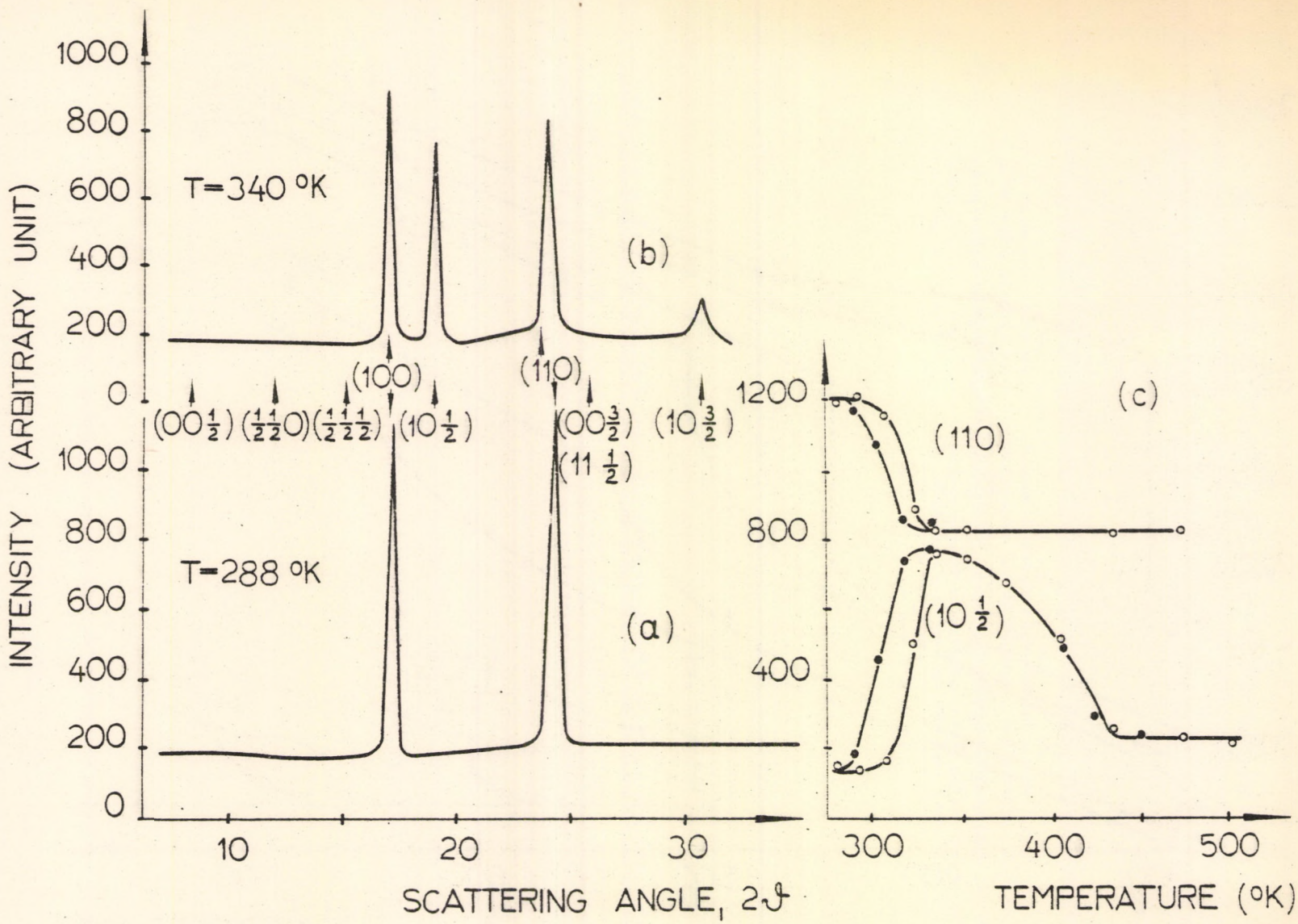

Fig. 5

Neutron diffraction results for $Mn_{2,83}Pt_{1,17}$. /a/ Pattern at 288° K. /b/ Pattern at 340° K. /c/ Temperature dependence of the $(10\frac{1}{2})$ and (110) reflections indexed in the original unit cell.

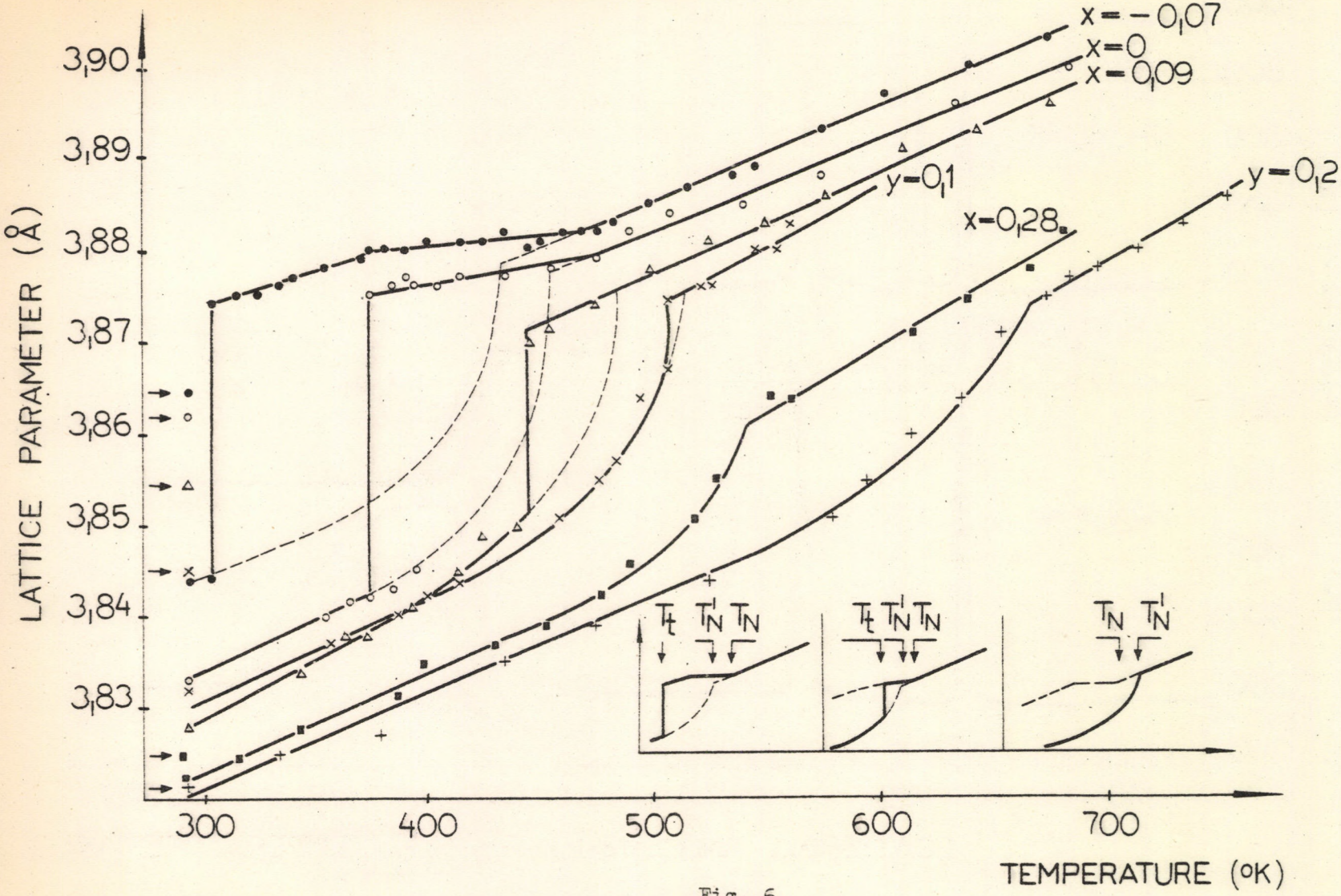

Fig. 6

Temperature dependence of the lattice parameter for samples with different values of x and y in the $Mn_{3+x}Pt_{1-x}$ and $Mn_3Pt_{1-y}Rh_y$ systems. The values at room temperature marked by arrow are extrapolated from the paramagnetic state

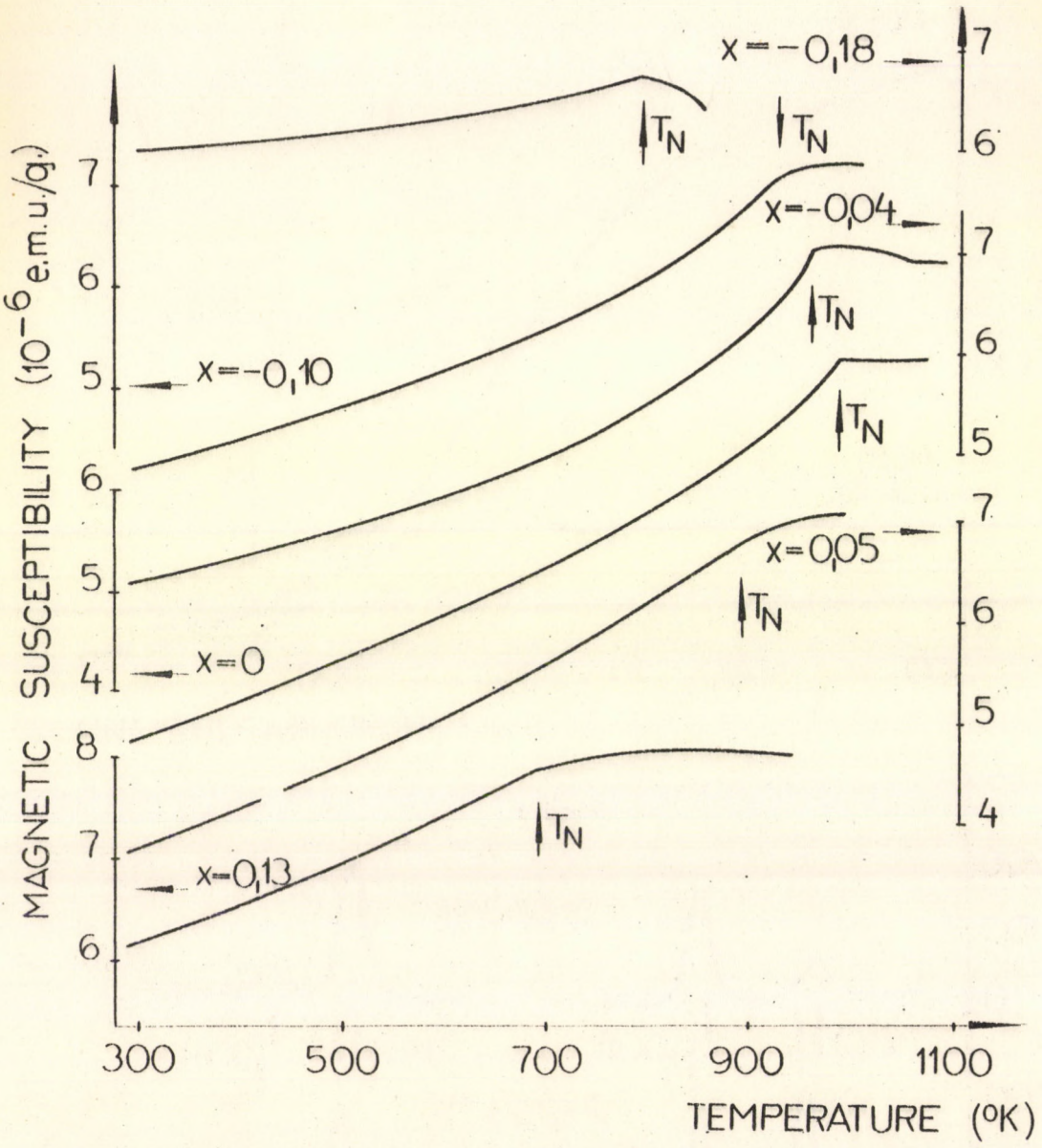

Fig. 7

Temperature dependence of the magnetic susceptibility for various alloys in the $Mn_{1+x}Pt_{1-x}$ system. The values of T_N marked in the figure were obtained by neutron diffraction

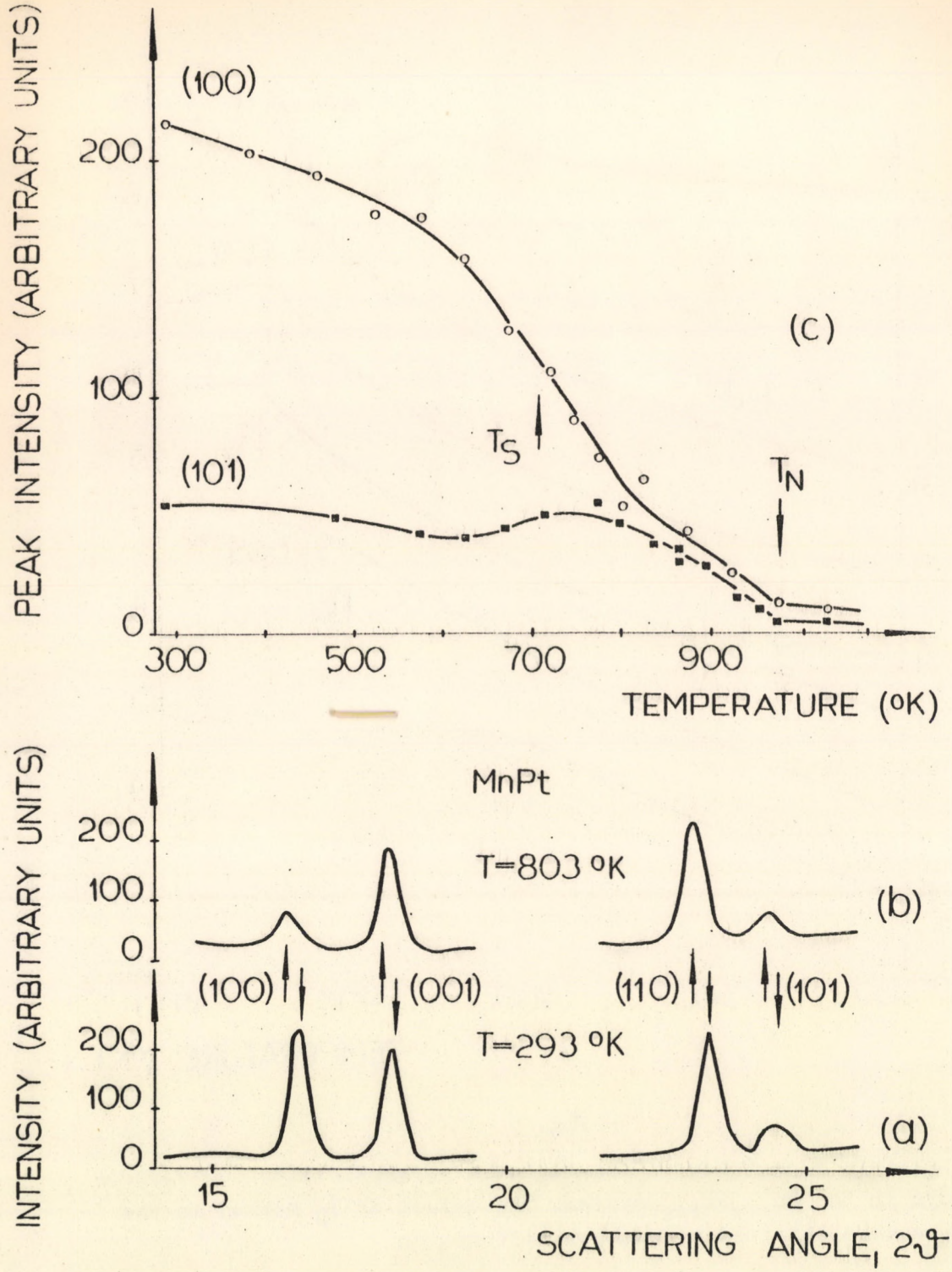

Fig. 8

Neutron diffraction results for MnPt. /a/ Pattern at 293° K. /b/ Pattern at 803° K. /c/ Temperature dependence of the (100) and (101) peak intensities

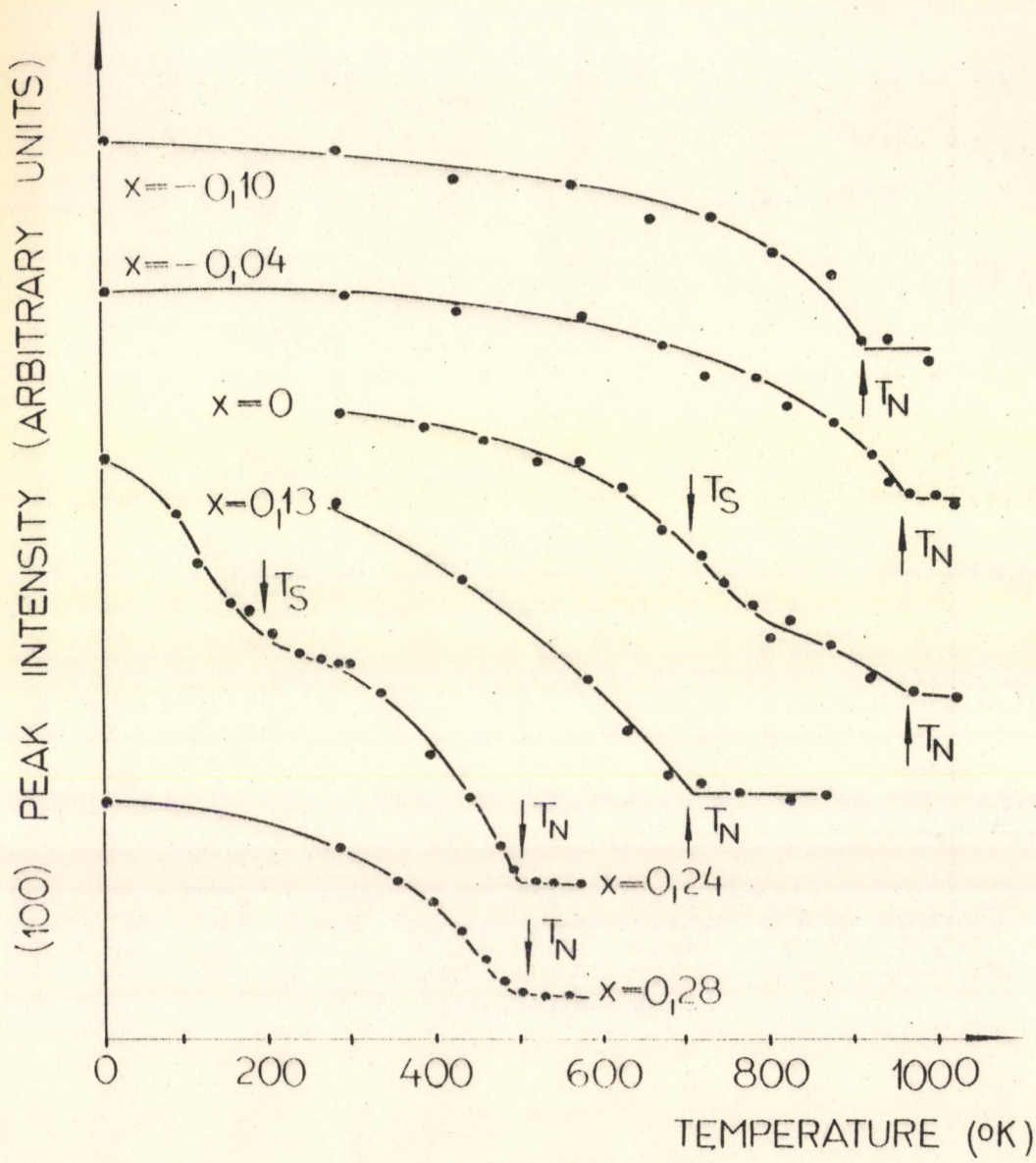

Fig. 9
Temperature dependence of the (100) peak intensity for various alloys in the $Mn_{1+x}Pt_{1-x}$ system

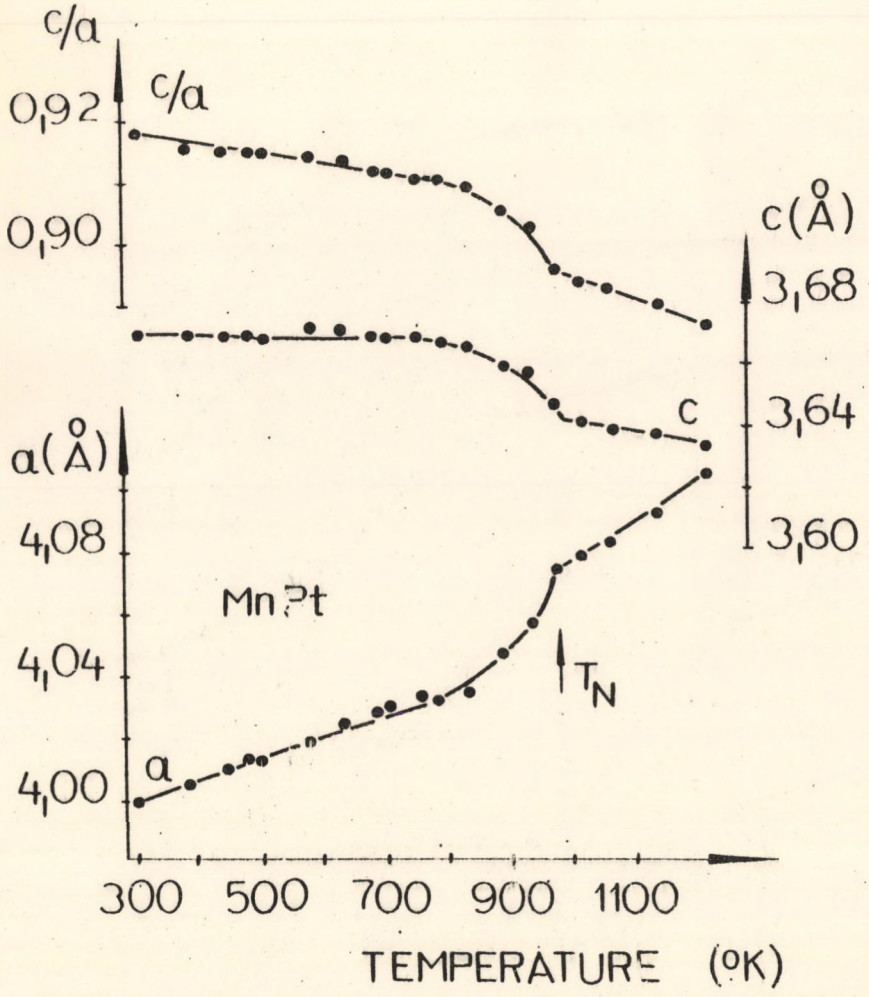

Fig. 10
Temperature dependence of the lattice parameters a and c in MnPt

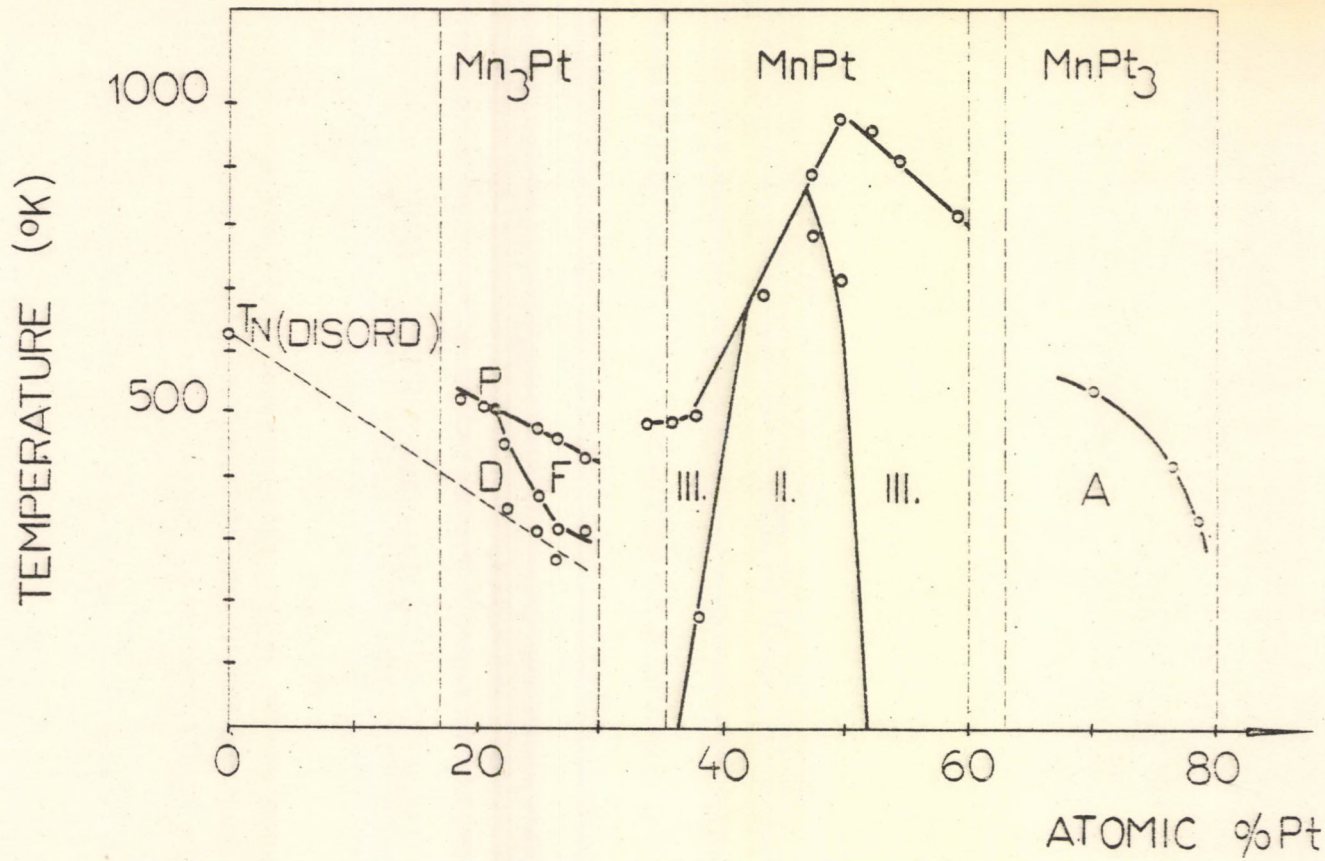

Fig. 11

Magnetic phase diagram of the Mn-Pt system. The letters denoting the stability regions of the various magnetic structures refer to the models of Figs. 1-2.

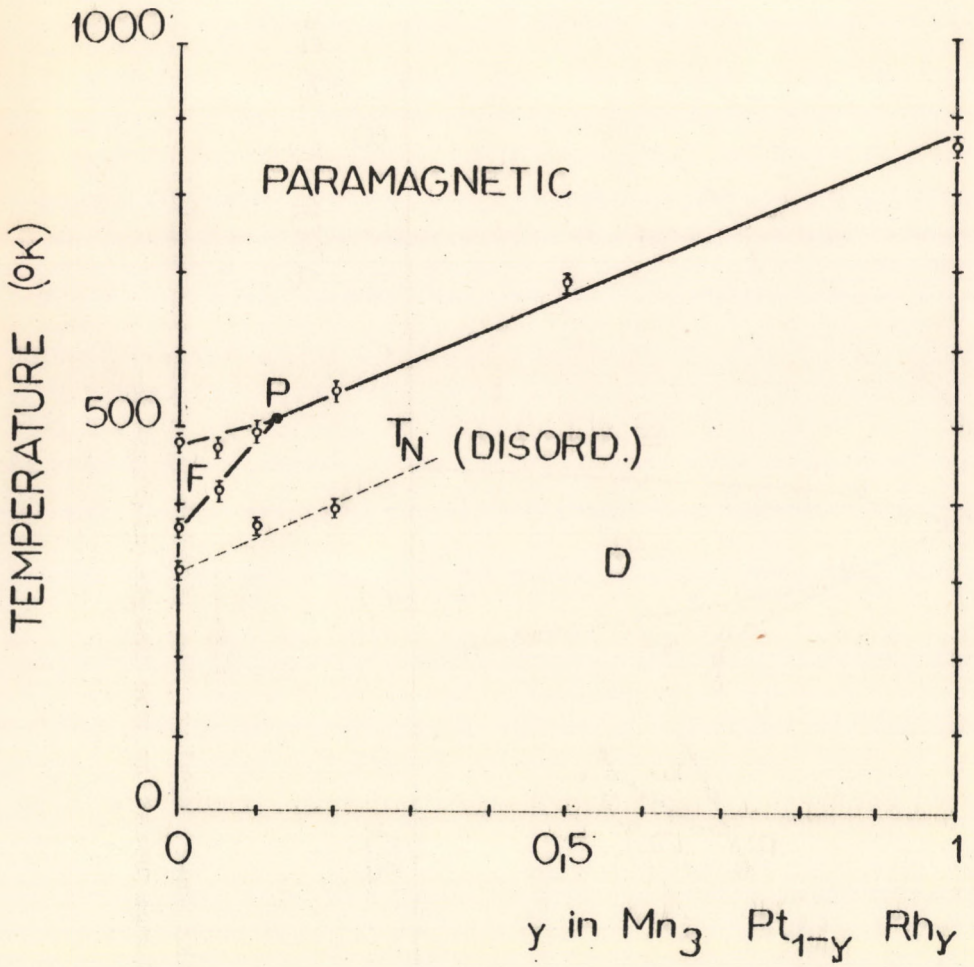

Fig. 12

Magnetic phase diagram of the $Mn_3Pt_{1-y}Rh_y$ system. The letters denoting the stability regions of the various magnetic structures refer to the models of Fig. 1.

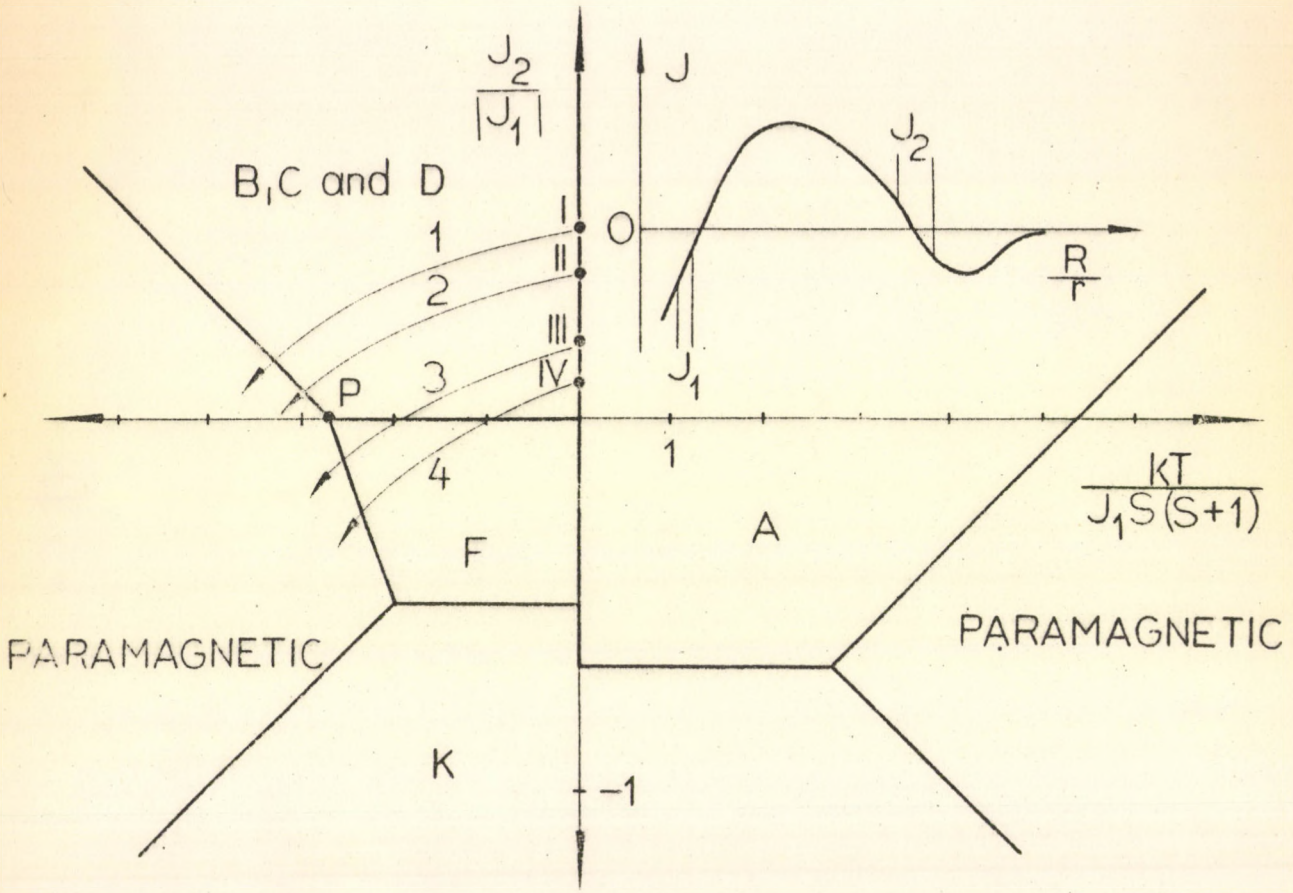

Fig. 13

Theoretical phase diagram in the molecular field approximation for the Mn_3Pt region. A, B, C, D and F refer to the structures of Fig. 1, while K denotes a collinear antiferromagnetic structure with eightfold magnetic unit cell. Figure /a/ shows the magnetic interactions located on a Bethe-Slater type qualitative curve

Printed in the Central Research Institute for Physics, Budapest

Kiadja a KFKI Könyvtár- és Kiadói Osztály
o.v. Farkas Istvánné

Szakmai lektor: Pál Lénárd
Nyelvi lektor: Kovács Jenőné

Példányszám: 150 Munkaszám: 3382
Budapest, 1968. február 8.

Készült a KFKI házi sokszorositójában
F.v.: Gyenes Imre